Proc. Indian Acad. Sci. (Earth Planet. Sci.), Vol. 101, No. 1, March 1992, pp. 47–66.

Simulation of barotropic wind-driven circulation in the upper layers of Bay of Bengal and Andaman Sea during the southwest and northeast monsoon seasons using observed winds

N BAHULAYAN and A S UNNIKRISHNAN

Physical Oceanography Division, National Institute of Oceanography, Dona Paula, Goa 403 004, India

MS received 25 October 1990; revised 2 December 1991

Abstract. A two-dimensional, nonlinear, vertically integrated model was used to simulate depth-mean wind-driven circulation in the upper Ekman layers of the Bay of Bengal and Andaman Sea. The model resolution was one third of a degree in the latitude and longitude directions. Monthly mean wind stress components used to drive the model were obtained from the climatic monthly mean wind data compiled by Hastenrath and Lamb. A steady-state solution was obtained after numerical integration of the model for 15 days. The sensitivity of the model to two types of open boundary conditions, namely, a radiation type and clamped type, was tested. A comparison of simulated results for January with available ship drift data showed that the application of the latter along the open boundary could reproduce all the observed features near the boundary and the interior of the model domain. The model was integrated for 365 days to study the circulation during the southwest and northeast monsoon seasons. The model was successful in simulating the broad features of circulation including gyres and eddies observed during both the seasons, the development of north equatorial current during the northeast monsoon period and eastward moving monsoon drift current up to 90°E during the southwest monsoon season. During the latter season, two anticyclonic gyres were observed in the central and the southern parts of the Bay. A cyclonic type of circulation was prevalent in the central and western parts of the Bay of Bengal during the northeast monsoon months of November and December. The simulated western boundary current along the east coast of India, flows northward and southward during the southwest and northeast monsoon seasons respectively. It is presumed that this western boundary current, simulated during both the seasons, is locally wind-driven.

Keywords. Barotropic circulation; wind-driven layer; seasonal variability; Bay of Bengal; numerical model; boundary conditions; steady-state solution.

1. Introduction

Circulation in the Bay of Bengal and the Andaman Sea (BBAS) (figure 1), the northeastern arm of the Indian Ocean, is mainly controlled by the prevailing monsoon winds, which reverse semi-annually, blowing from the northeast during the northern hemisphere winter and from the southwest during summer. This semi-annual reversal of wind field causes a corresponding reversal of circulation in the upper layers of the water body. The surface circulation in the northern Bay of Bengal (BB), Andaman Sea and along the east coast of India is also modified by enormous amounts of freshwater discharges to its shores by various rivers (Panakala Rao and Sastry 1981). The six-monthly reversal of the wind field over the area coupled with variations of freshwater discharges to the coastal regions over the year and the complex tidal oscillations within the Bay make the study of circulation in the BBAS very challenging.

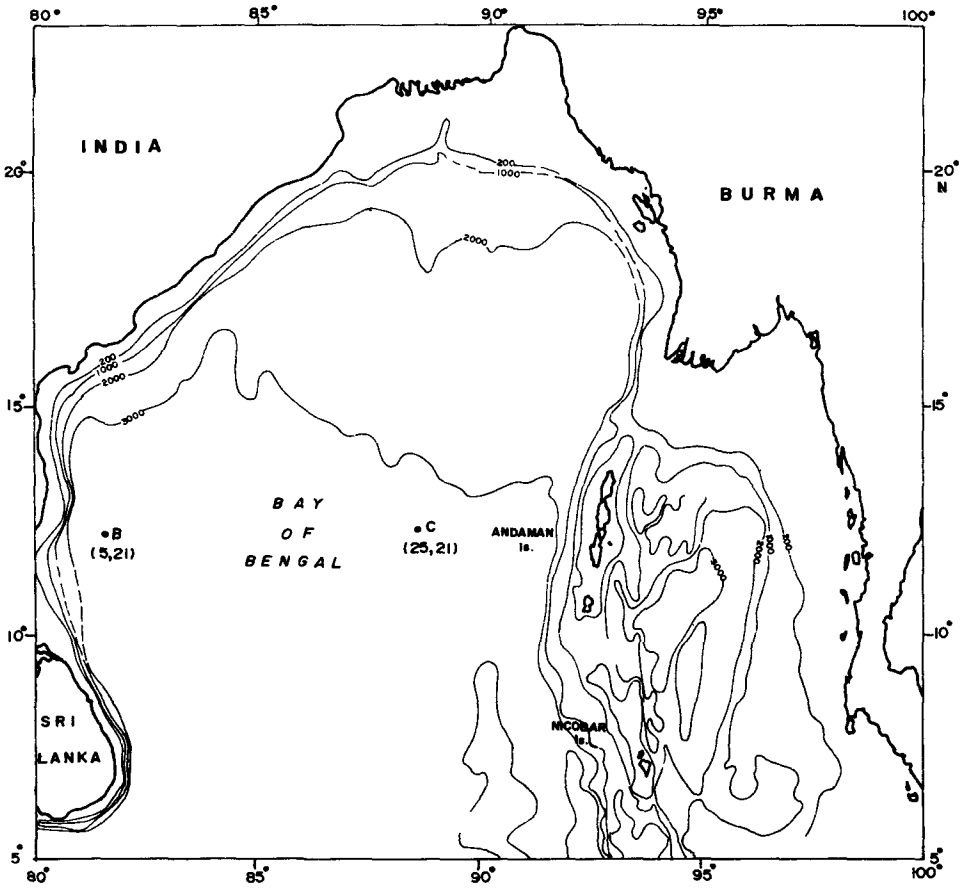

Figure 1. Geographic location map of Bay of Bengal and Andaman Sea with bathymetric contours.

Scientists of the National Institute of Oceanography have been collecting and analysing oceanographic data of BB during the past few years to study its steady-state circulation and water mass structure. However, there have been no serious efforts to model the circulation in the Bay in response to the above mentioned forces, except the modelling of tides and storm surges (Johns *et al* 1981; Murty 1984). In the present study, an attempt was made to model the depth-mean circulation in the upper wind-driven layers of BBAS using climatological wind as the forcing function. A more satisfactory simulation would involve variation of flow with depth particularly in view of the large seasonal freshwater inflow. A fully three-dimensional model that incorporates thermohaline forcing and river discharges will be developed later. The present paper is the first attempt to model the circulation in the Bay of Bengal.

The currents in the Bay of Bengal are less documented than those in the Arabian Sea. Luther and O'Brien (1985) developed a model of seasonal circulation in the Arabian Sea forced by observed winds by using nonlinear reduced gravity transport equations to simulate the seasonal circulation in the Arabian Sea. The model reproduced well the Somali current system including its two gyre circulation pattern. Initial studies on the currents in the Bay of Bengal were carried out by Lafond and

coworkers (Lafond and Boreswara Rao 1954; Lafond 1958; Lafond and Lafond 1968). Varadachari *et al* (1968) prepared the circulation pattern in the upper 500 metres of the northern BB between 9° and 16°N latitudes during the southwest monsoon period based on geopotential anomalies. Neuman (1974) studied the circulation pattern in BB and found that anticyclonic oceanic circulation is prevalent during the winter months. Cutler and Swallow (1984) illustrated a northward flowing current along the western boundary of the Bay of Bengal from February to June based on 10-day averages of historical ship drift. Shcherbinin *et al* (1979), during a hydrographic survey in 1979 off Madras, located the core of a western boundary current in BB between 81° and 82°E. Legeckis (1987) identified a western boundary current in the Bay of Bengal in late February through satellite images.

Cox (1970) was the first to develop a numerical model of the Indian Ocean including its marginal seas, the Bay of Bengal and Arabian Sea. The model was three-dimensional and had the observed shape of the Indian Ocean with respect to lateral and bottom boundaries. The model equations were solved by an extended numerical integration. The total period of integration was two centuries. Cox's model, driven by observed seasonal winds, temperature and salinity, could reproduce the major features of circulation in BB during August and February, but it could not simulate the small-scale features of circulation such as gyres and small-scale eddies, probably due to the use of seasonal winds, temperature and large mesh size used (1° resolution) in the model.

Many reports have appeared on wind-driven circulation since the pioneering studies of Ekman. His analytical theory of wind-driven circulation was aimed at describing quantitatively the structure of circulation in the upper layers of the ocean based on certain idealized assumptions such as no boundaries for the ocean, infinitely deep water, homogenous water body etc. Our objective in the present study was to simulate the "depth-mean circulation" in the upper layers of BBAS using a depth-averaged model for which the main forcing is observed wind. The depth of the wind-driven layer, function of wind speed and latitude of the region, was computed using an empirical relation suggested by Ekman.

The hydrodynamic model to simulate depth-mean circulation in the upper layers of BBAS during southwest and northeast monsoon seasons was earlier reported (Bahulayan and Vardachari 1986). The same model was used in the present study to simulate the circulation, but was driven by observed monthly mean winds. The model is briefly described in the following sections. Monthly mean wind fields compiled on 1° squares over a 60-year period (Hastenrath and Lamb 1979) were used to drive the model, which was integrated for 365 days to study the seasonal evolution of circulation in BBAS. The sensitivity of the model to two different open boundary conditions was tested. The distribution of the computed wind stress components, simulation results for the southwest and northeast monsoon seasons and their comparison with available information on currents are reported in what follows.

2. Numerical model

2.1 *Governing equations and boundary and initial conditions*

We used rectangular cartesian co-ordinates, in which the x, y and z axes pointing towards east, north and vertically upward respectively were considered. The displaced

level of sea surface is given by $z = \eta(x, y, t)$ and the bottom of the wind-driven layer corresponds to $z = -h(x, y)$. The vertically integrated equations used to describe the motion of a homogenous ocean on a β plane are given below. Equation (1) is the continuity equation and (2) and (3) are the momentum equations in x and y directions respectively.

$$\frac{\partial \eta}{\partial t} + \frac{\partial \bar{u}}{\partial x} + \frac{\partial \bar{v}}{\partial y} = 0, \tag{1}$$

$$\frac{\partial \bar{u}}{\partial t} + \frac{\partial}{\partial x}(u\bar{u}) + \frac{\partial}{\partial y}(v\bar{u}) + f\bar{v} = -g(\eta + h)\frac{\partial \eta}{\partial x} + \frac{\tau_x^\eta}{\rho_w} - \frac{k\bar{u}}{(\eta + h)}\left[\frac{\bar{u}^2}{(\eta + h)^2} + \frac{\bar{v}^2}{(\eta + h)^2}\right]^{\frac{1}{2}}, \tag{2}$$

$$\frac{\partial \bar{v}}{\partial t} + \frac{\partial}{\partial x}(u\bar{v}) + \frac{\partial}{\partial y}(v\bar{v}) + f\bar{u} = -g(\eta + h)\frac{\partial \eta}{\partial y} + \frac{\tau_y^\eta}{\rho_w} - \frac{k\bar{v}}{(\eta + h)} \times \left[\frac{\bar{u}^2}{(\eta + h)^2} + \frac{\bar{v}^2}{(\eta + h)^2}\right]^{\frac{1}{2}}, \tag{3}$$

where u and v are the prognostic variables defined by

$$\bar{u} = u(\eta + h) \text{ and } \bar{v} = v(\eta + h). \tag{4}$$

The other symbols denote t, time; η, elevation of sea surface with reference to its undisturbed-surface; u, v, depth-averaged velocities in the x and y directions respectively; f, Coriolis parameter which is assumed to vary linearly with latitude ($f = f_0 + \beta y$); f_0, the value of Coriolis parameter at the southern boundary of the domain ($1{\cdot}526 \times 10^{-5}\,s^{-1}$); β, variation of Coriolis parameter with latitude ($\partial f/\partial y$); g, acceleration due to gravity ($9{\cdot}81\,m{\cdot}s^{-2}$); ρ_w, density of sea water ($1{\cdot}02 \times 10^3\,kg{\cdot}m^{-3}$); τ_x^η, τ_y^η, x and y components of wind stress and K, bottom friction coefficient ($1{\cdot}1 \times 10^{-3}$).

In (2) and (3), the bottom friction was parameterized in terms of a quadratic friction law. The model area extends between the longitudes 80° and 98°E and latitudes 6° and 22·5°N. The southern boundary along 6° was an open boundary. The western, northern and eastern boundaries of the model domain were closed and a zero-normal flux condition of $u = v = 0$ was applied depending on the orientation of the stair step line segments. Thus $v = 0$ was applied on those straight line segments that were parallel to x-axis and $u = 0$ was applied on those straight line segments that were parallel to y-axis. The initial condition was $u = v = \eta = 0$ at $t = 0$.

Linearized version of the depth-integrated equations of motion and continuity was applied to simulate depth-mean currents in a wide variety of bays, coastal seas and straits, where depths as high as 3000 m were observed. O'Brien(1971) used a vertically-averaged model to simulate the wind-driven circulation in the north Pacific. Fandry (1981, 1982) simulated the wind-driven circulation in the Bass strait using depth-integrated equations. He used a constant maximum depth of 500 m at all grid points, where the actual depths exceeds 500 m. It is to be mentioned that greater caution should be exercised while applying shallow water equations in deeper oceanic areas. The simulated circulation in such cases would be definitely quite less than what is normally observed. Further, care should be taken to select the appropriate bottom

friction coefficient, since the frictional dissipation at the bottom of the Ekman wind-driven layer is much less than in a solid boundary of the sea bed. We, therefore, used a low value for the friction coefficient which was obtained through numerical experiments.

The specifications of correct open sea boundary condition are still a matter of dispute among scientists the world over. The effect of large-scale ocean circulation in the rest of the ocean basin must be brought in at the open sea boundary through the specification of boundary conditions. This essentially includes the specification of transports in and out of the region or prescribing baroclinicity and sea surface elevation along the open boundaries. The observed data on the above quantities on a synoptic scale, if available, are the best for the above purpose. It is practically impossible to obtain, on a synoptic basis, information on transports or sea surface elevation. Another alternative is to specify a radiation-type boundary condition along the open sea boundary by which transients generated inside the region are allowed to be transmitted outwards. In this paper, we use the following radiation boundary condition (Heaps 1973; Johns *et al* 1981).

$$v + (g/h)^{\frac{1}{2}}\eta = 0 \text{ at } y = 0. \tag{5}$$

From equation (5), a relation for η at the open boundary was derived and updated at each time-step of integration. For a purely wind-driven flow, the condition of sea surface elevation $\eta = 0$ can also be applied, if the sea is contiguous with deep ocean (Fandry 1981). We conducted a few numerical experiments with this model using both the above mentioned boundary conditions. It was found that the clamped boundary condition was more effective in realistically simulating the circulation inside the Bay. The present results are based on the application of clamped open sea boundary condition ($\eta = 0$).

2.2 *Computation of the depth of wind-driven layer*

The hydrodynamic equations (1) to (3) were derived assuming that vertical variations of flow caused by vertical density stratification are negligible. The Bay of Bengal exhibits considerable vertical variations in density and hence it would be unrealistic, if the depth-mean wind-driven circulation in BBAS is simulated using the above mentioned vertically integrated equations and actual depths. Therefore, in the present study, we considered only the upper homogeneous layer, which is affected by wind for the simulation of the depth-mean circulation. The approximate thickness of the upper homogeneous wind-driven Ekman layer D_E, to a first approximation, is a function of wind speed and latitude of the region and can be expressed as (Pond and Pickard 1983)

$$D_E = 4{\cdot}3\, W/(\sin\phi)^{\frac{1}{2}} \text{ metres } (W \text{ in ms}^{-1}), \tag{6}$$

where W is the wind speed in m/s and ϕ is the latitude of the region. If the vertical eddy viscosity coefficient is accurately known, D_E can be calculated using the following relation (Murty 1984).

$$D_E = \sqrt{2\nu}/f, \tag{7}$$

where f is the Coriolis parameter and v the vertical eddy viscosity coefficient. Very often, values for D_E have been compared with the depth of the mixed layer. In fact, this assumption is not quite correct. The mixed layer depth depends on the past history of the wind field in the locality more than on the wind speed at the time of observation. It also depends on the heat exchange through the sea surface, the process of upwelling and sinking and also on the internal waves. In the case of Bay of Bengal, there is a month-to-month variation in the mixed layer depth due to heavy freshwater fluxes from the rivers adjoining the east coast of India. Since wind field is the main forcing in our model, we decided to use relation (6) to compute the depth of the wind-driven layer.

Monthly mean wind field compiled by Hastenrath and Lamb (1979) on 1° squares for the Indian Ocean was used to compute the depth of wind-driven layer. Since the model resolution was one third of a degree in x and y directions, the monthly mean wind field also was linearly interpolated in space to one third of a degree. The depth of wind-driven layer at each grid point for each month was computed using relation (6). If the actual depth at a grid point is less than the computed depth of the wind-driven layer, then the actual depth is taken for the numerical simulation.

The depth of the wind-driven layer was proportional to the wind speed (equation (6)) when it was less than the ocean depth. This relation is applicable to time-varying wind conditions and hence we have different depths of wind-driven layer for each month. Equations (1) to (3) were integrated over this depth of wind-driven layer.

2.3 *Computation of wind stress*

The monthly mean wind stress components computed from the monthly mean wind field are the main forcings for the model. The resultant wind stress $|\bar{\tau}|$ was first computed using the following relation.

$$|\bar{\tau}| = C_D \rho_{\text{air}} |\bar{V}|^2, \tag{8}$$

where C_D is the drag coefficient of air, ρ_{air} is the density of air and $\bar{V}$ the monthly mean resultant wind speed. C_D is a linear function of the resultant wind speed and the following relation given by Wu (1980) was used for its calculation

$$C_D = (0{\cdot}8 + 0{\cdot}065\,|\bar{V}|)10^{-3}. \tag{9}$$

The monthly mean wind stress components τ_x^η and τ_y^η were then calculated with the aid of the following relation

$$\tau_x^\eta = |\bar{\tau}| \sin \bar{\alpha}, \quad \tau_y^\eta = |\bar{\tau}| \cos \bar{\alpha}. \tag{10}$$

In (10), $\bar{\alpha}$ is the mean wind direction vector measured with respect to the geographic north. The wind stress components, which are taken positive to the east and north respectively, were computed for each month using (10) and their distribution during the southwest monsoon and the northeast monsoon seasons is mentioned briefly in § 4.

3. Numerical procedure

The hydrodynamic equations (1) to (3) were solved numerically subject to the boundary and initial conditions mentioned above on a 55 × 50 finite difference mesh by means

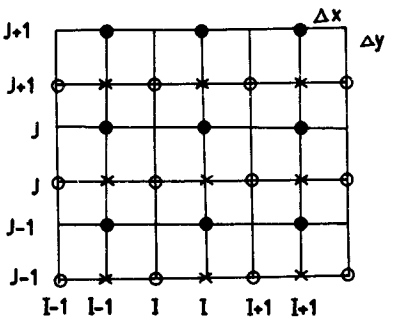

Figure 2. Staggered grid finite difference mesh used in the discretization of governing equations. Points marked ●, ○ and × are u, v and η points respectively.

of an explicit scheme. The mesh is staggered in space (figure 2). The grid resolution is 33·5 km and 36·5 km in the x and y directions respectively. The resultant current speed and direction were computed at the u points. For this purpose, v values were interpolated to the u points by taking an arithmetic means of the four values of v surrounding a u point.

The hydrodynamic model, forced with the mean wind stress components for January, was integrated from the rest, beginning at 0000 hrs on 1 January. A time-step of 600 s was chosen for the numerical integration which satisfied the Courant-Friedrichs-Lewy (CFL) stability criterion given by $\Delta t \leqslant (\Delta x, \Delta y)\,(2gh)^{-1/2}$, where Δx and Δy are the space steps in x and y directions and h the maximum depth of the wind-driven layer. The model fields spin up very fast and a steady-state circulation was attained after approximately 15 days of numerical integration. Keeping the wind stress components for January constant, the integration was continued for one month. The simulated model fields at the end of January (31st day) were taken as the initial condition for February and the model was again integrated till the end of February (28th day), using the mean wind stress components of February as the forcing. The sudden change of wind field at the beginning of February generated initial transients in the solutions, which were completely dissipated through friction after approximately 15 days of numerical integration. By replacing the wind forcing at the beginning of each month with the corresponding monthly mean wind stress components and using the solution obtained at the end of the previous month as the initial condition for the subsequent month, integration of the model equations was continued till the end of December to study the complete seasonal variability of circulation in BBAS. We used a low value for the bottom friction coefficient ($1{\cdot}1 \times 10^{-3}$) and the same was obtained through tuning the model with various values. Normally, in shallow water models, the bottom friction coefficient of the order of $2{\cdot}5 \times 10^{-3}$ is used. Since we have an artificial fluid bottom, where frictional dissipation is expected to be much less than that in a solid bottom and also that monthly mean wind-driven currents have low magnitudes, it is reasonable to use a low value for the bottom friction coefficient.

4. Results and discussion

4.1 *Steady-state solution*

As mentioned earlier, the model equations were integrated from the rest using the mean wind stress components for January as the forcing for a period of 31 days to

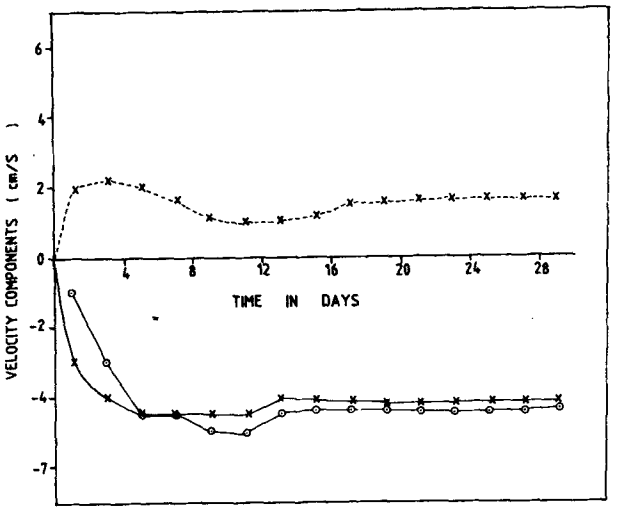

Figure 3. Time dependence of wind-driven velocity components at selected points in the model area (refer figure 1); ○–○ u component of velocity at B (5, 21); × – × u component of velocity at C (25, 21); × —— × v component of velocity at C (25, 21).

study the stability of solution. Two points B and C (figure 1) in the model domain, representing the coastal and open environments, were chosen to study the time dependence of wind-driven velocity components (figure 3). It was found that a steady state was attained at both the points between 13 and 16 days of integration of the model and thereafter the values remain constant till the 31st day of integration. The integration was also continued for subsequent months using the corresponding monthly mean wind stress components as forcing and it was found that a stable solution was obtained around the 15th of every month and no instability was noticed even after a few months of integration.

4.2 *Sensitivity of the model to open boundary conditions and simulation of circulation during January*

Two numerical experiments were performed to test the sensitivity of the model to open boundary conditions. In the first, a radiation type of boundary condition as definied by equation (5) was applied along the southern boundary of the model domain and the model was integrated, using the mean wind stress components for January as forcing, from the remaining for 31 days beginning 0000 hrs on January of the year. The steady-state circulation generated after 31 days of integration is shown in figure 4. In the second experiment, an open boundary condition of zero-surface elevation was applied along the southern boundary and the model was integrated using the same wind forcing for 31 days, beginning 0000 hrs on 1 January of the year. The steady-state circulation generated (31st January) is shown in figure 5. A comparison of figures 4 and 5 shows that radiation boundary condition could not reproduce realistically the currents near the southern boundary. In fact, the simulated currents near the boundary are opposite to the observed currents (Culter and Swallow 1984) and wind direction. This effect could be seen up to a width of 1° latitude from the southern boundary. The overall circulation features in the central and northern parts of the model area

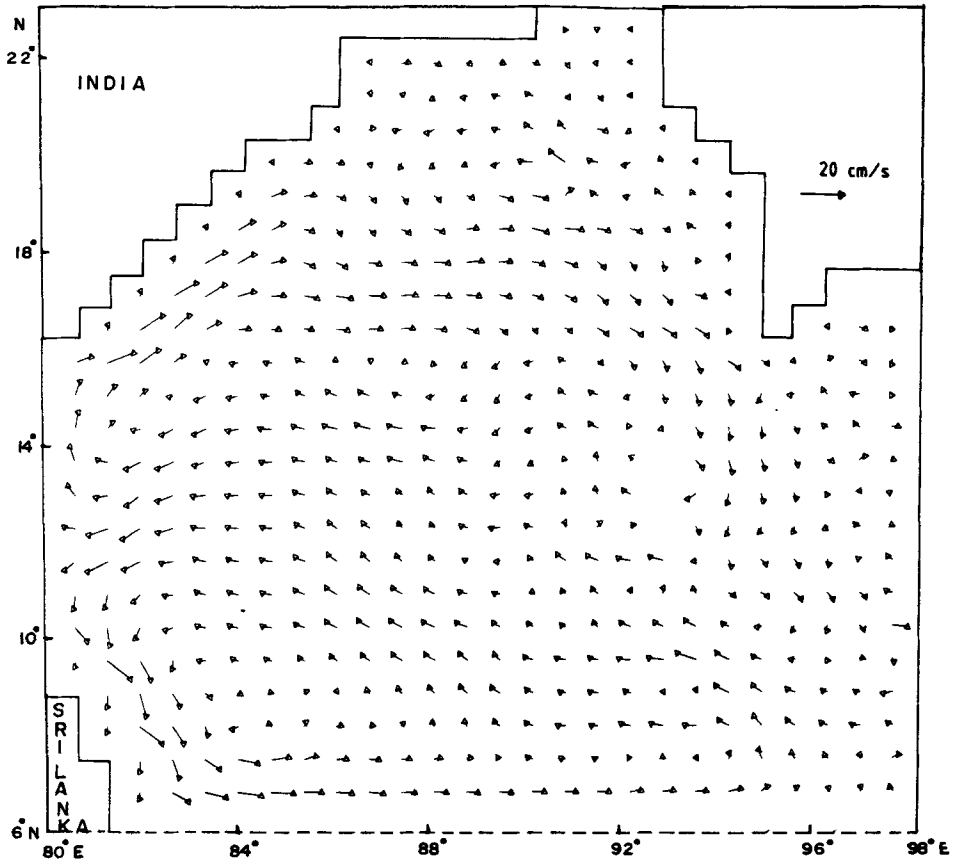

Figure 4. Simulated depth-mean circulation on the 31st day of January, when radiation boundary condition was applied along the open boundary.

in both the numerical experiments are analogous. The open boundary condition of zero sea surface elevation could reproduce well the broad features in the whole model area. Hence, we use the same open boundary conditions for the simulation of seasonal circulation in BBAS.

4.3 *Spatial distribution of monthly mean wind stress components*

The methodology for computation of monthly mean resultant wind stress and its components was given above. Since wind stress components are the main external forcing in the model, we briefly present the distribution of wind stress components during two seasons.

(a) *Southwest monsoon season (June–July)*: During June, the intensity of the southwest monsoon is considerably increased and mean wind speeds of the order of 7–8 m/s are observed throughout the model area. Therefore, magnitudes of both the x and y components of wind stress are high, with maximum values of the order of 0·075 Pa found in the central and western parts of the Bay (figures 6a and 6b). During July,

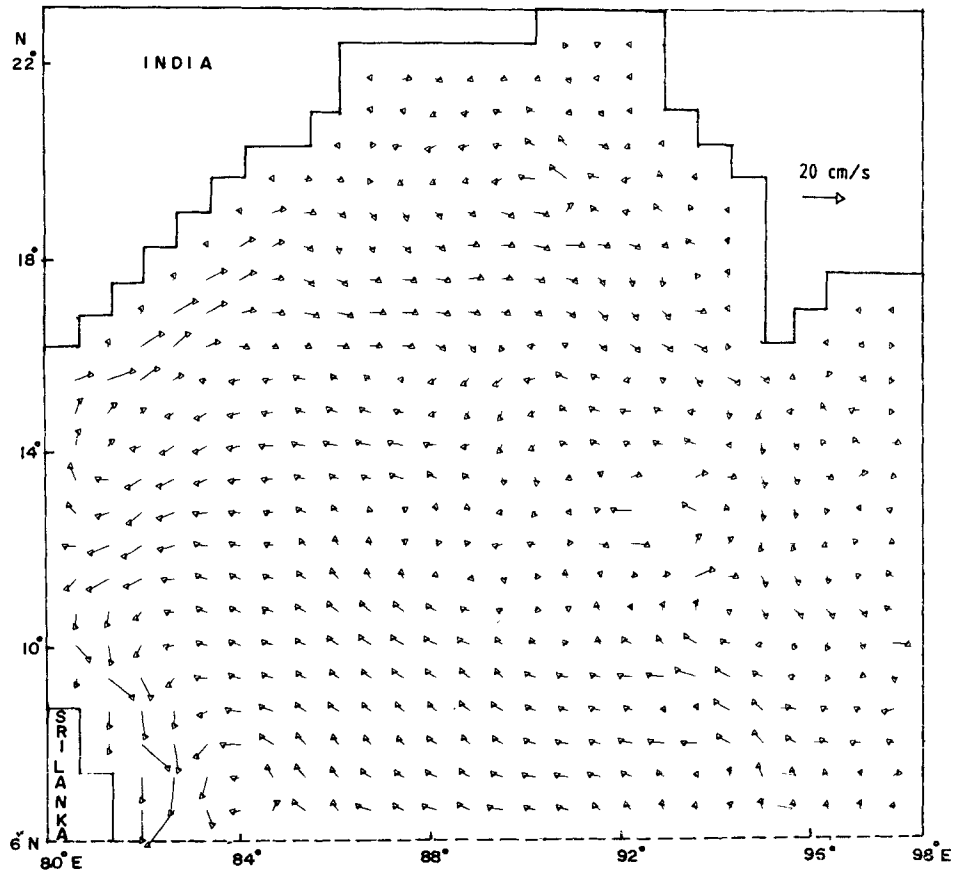

Figure 5. Simulated depth-mean circulation on the 31st day of January, when open boundary condition of zero surface elevation was applied.

the wind stress distribution is similar to that of June, with slightly higher magnitudes found than that of June (figures 6c and 6d).

(b) *Northeast monsoon season (November–December)*: By November, the change in the direction of winds from southwest to northeast is complete and the winds are northeasterly throughout the Bay of Bengal. The x and y components of wind stress have maximum values in the western and central parts of the BB (figures 6e and 6f). During December, the northeast monsoon is more intensified and wind speeds of the order of 5–6 m/s are observed in the central part of the BB. The x and y components of wind stress (figures 6g and 6h) are found to be maximum in the western part of the Bay ($-0{\cdot}035$ Pa).

5. Results of simulation of seasonal circulation and their comparison with observations

It was earlier mentioned in § 1 that a few observational studies on the circulation in BBAS give a steady-state structure of currents in only some selected regions of the

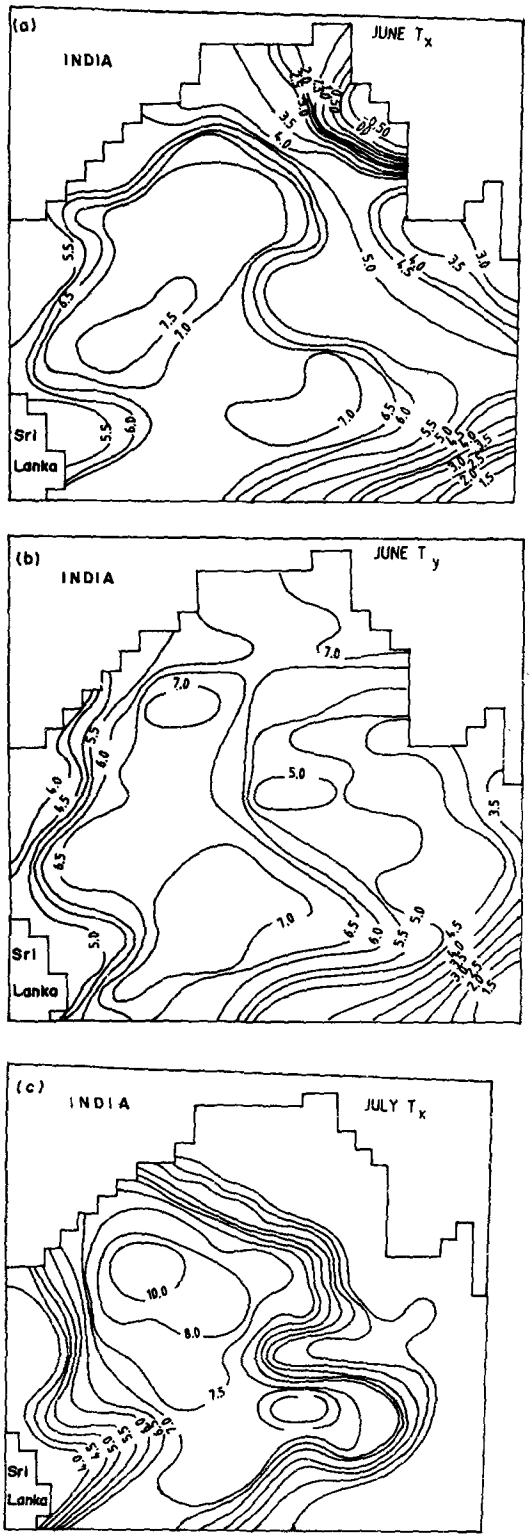
(a)
INDIA
JUNE T_x
Sri
Lanka
(b)
INDIA
JUNE T_y
Sri
Lanka
(c)
INDIA
JULY T_x
Sri
Lanka

Figure 6(a–c).

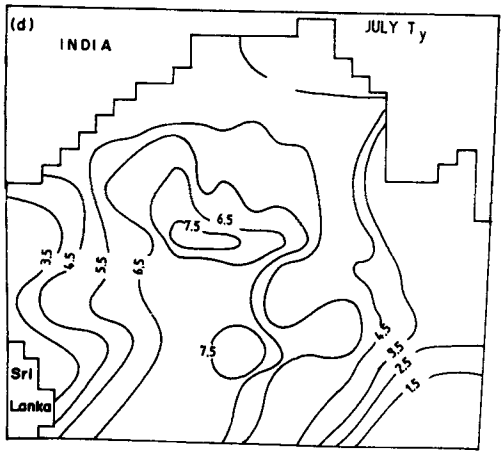
(d)
INDIA
JULY T_y
7.5
6.5
3.5
6.5
5.5
6.5
7.5
4.5
3.5
2.5
1.5
Sri
Lanka

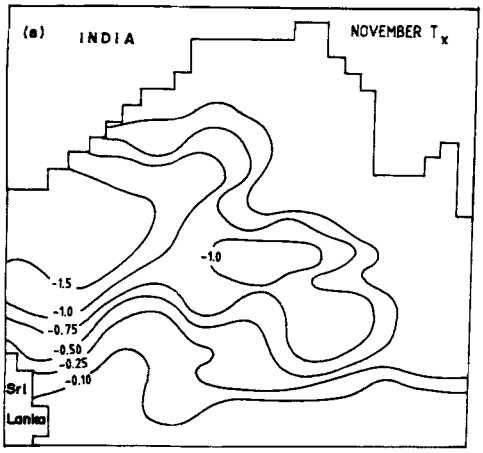
(e)
INDIA
NOVEMBER T_x
-1.0
-1.5
-1.0
-0.75
-0.50
-0.25
-0.10
Sri
Lanka

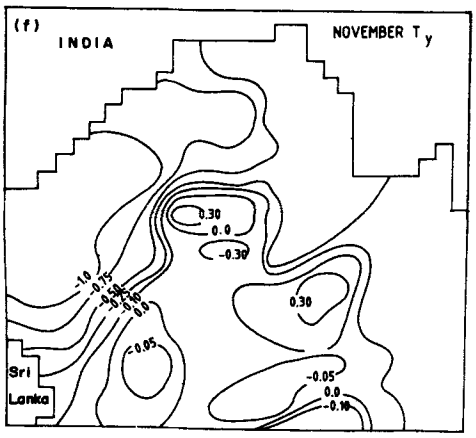
(f)
INDIA
NOVEMBER T_y
0.30
0.0
-0.30
0.30
-0.05
-0.05
0.0
-0.10
Sri
Lanka

Figure 6(d–f).

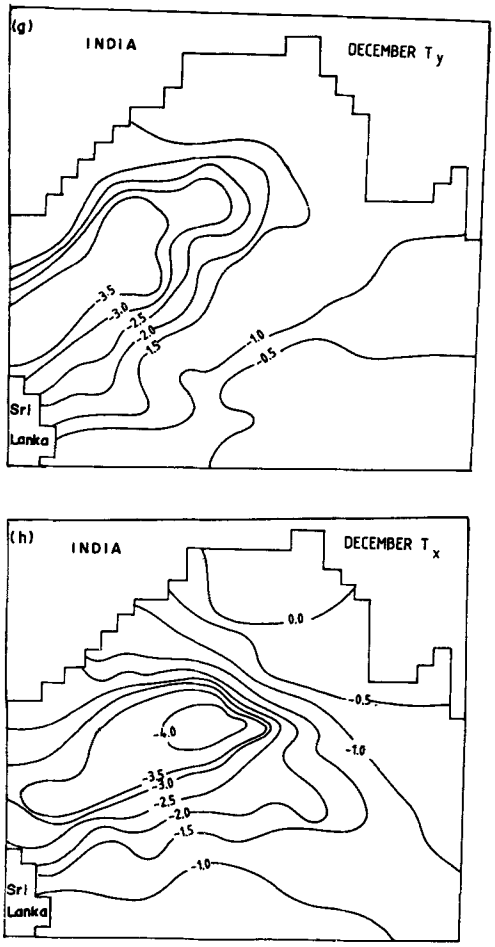

Figure 6(g–h).

Figure 6. Monthly mean x and y components of wind stress (0·01 Pa) for various months used as forcing for the model. **6a and 6b**—June; **6c and 6d**—July; **6e and 6f**—November; **6g and 6h**—December.

Bay of Bengal. It was difficult to compare the simulated results for the whole model area over the entire seasonal cycle with actual observations on currents. We, therefore, relied upon the compilation of surface currents, published in the form of atlases for the validation of model results. Historical data on surface currents are characterized by systematic and random errors. One of the earliest compilation of surface currents in the Indian Ocean is contained in the KNMI atlas (KNMI 1952). Its series of monthly charts is hardly adequate for showing the development of features with semi-annual periods such as equatorial jet. One of the latest and best compilation of Indian Ocean currents is contained in the atlas prepared by Cutler and Swallow (1984), hereafter referred to as CS Charts, in the form of 10-day averaged values on 1° squares. However, CS charts also suffer from several gross errors. There are points in the atlas where data are completely non-existent or adjacent points where very high differences in the current speed and direction are noticed. Meehl (1980) prepared the seasonal surface currents of the world ocean on a 5° grid. In this paper, we rely

mainly on the above two atlases for making a gross comparison of our model results with observations. In addition, other available information on currents in BB is also used to validate the model results. We discuss the simulated circulation during some selected months which represent typically the southwest monsoon and northeast monsoon seasons.

5.1 *Southwest monsoon season*

The simulated circulation towards the end of June and July is shown in figures 7 and 8 respectively. By the end of June, the southwest monsoon is fully set over the entire Indian subcontinent and the wind speeds are two to three times higher than those of the transition months, for example, October. The simulated currents are very intense, when compared to those in the previous months. The maximum current speed was observed along the Sri Lankan coast, where its value attained as high as 40 cm/s. Two broad anticyclonic gyres were formed in the central and southern parts of the Bay towards the end of June. In addition, a small cyclonic eddy was formed in the northeastern part of BB, where the magnitudes of currents were found to be as high as 30 cm/s. One branch of the strong current along the coast of Sri Lanka travels

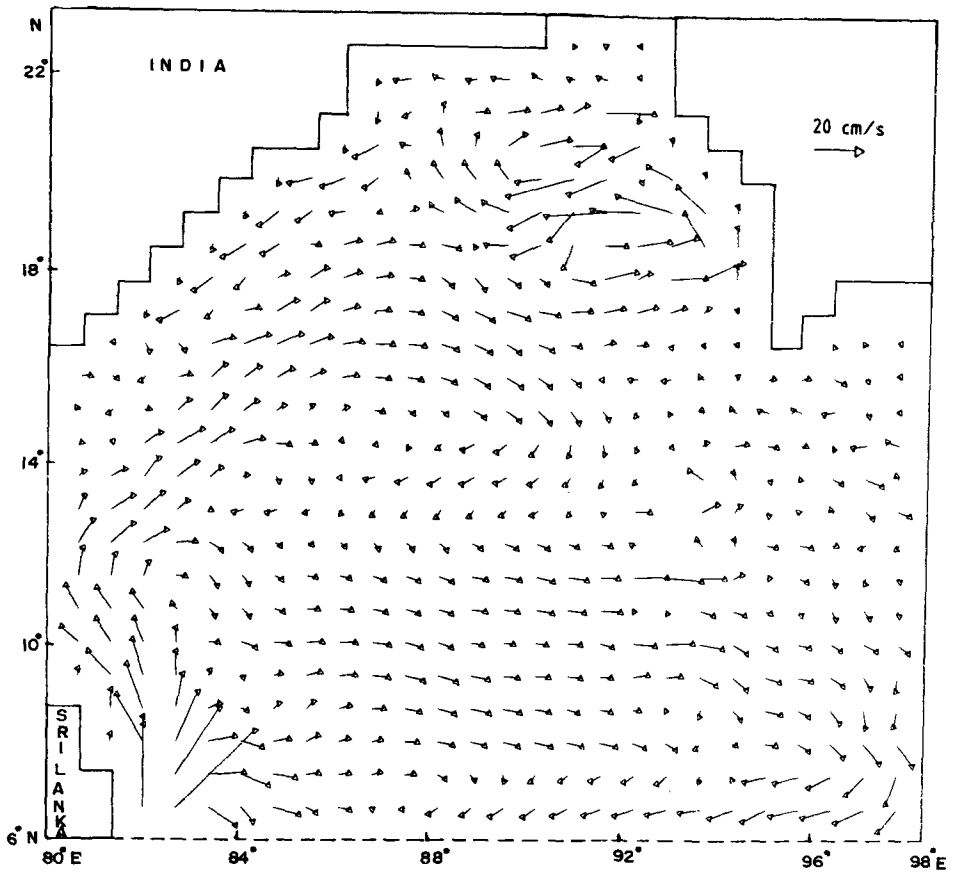

Figure 7. Simulated depth-mean currents for 30 June.

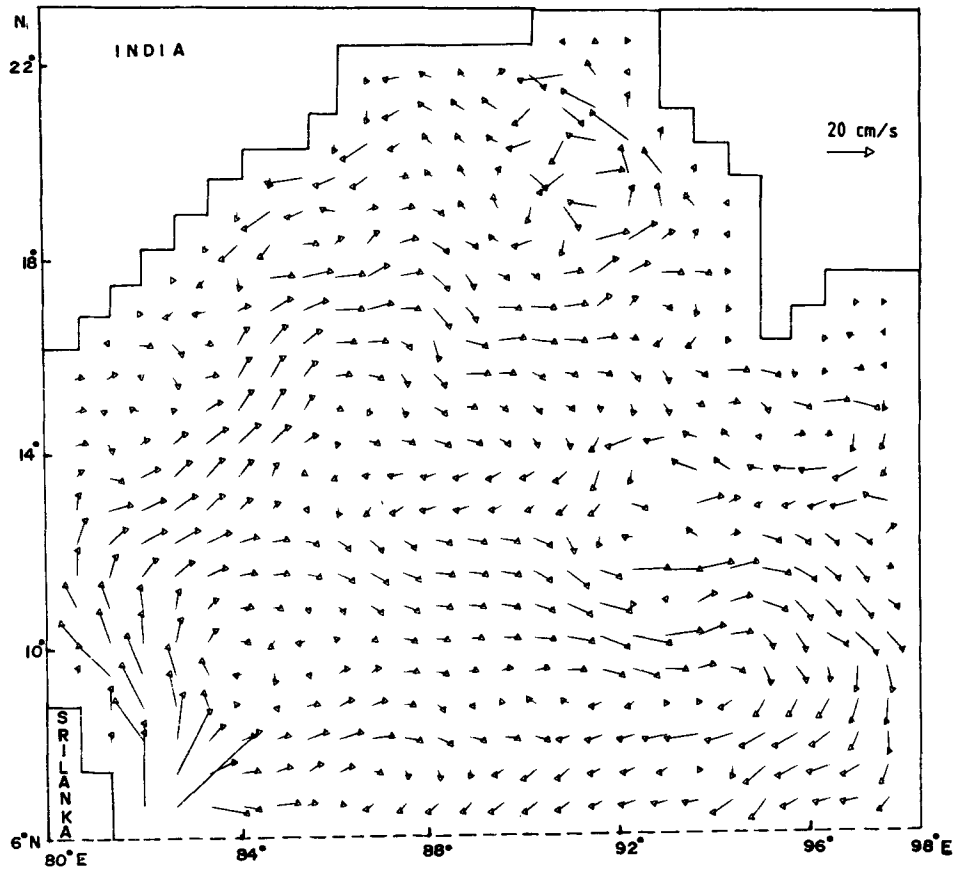

Figure 8. Simulated depth-mean currents for 31 July.

eastwards, turns southward on reaching the coasts of Thailand and then travels westwards to complete the anticyclonic gyre in the southern part of the Bay. The eastward moving current simulated in the southern part of the model is the monsoon drift current normally observed during the southwest monsoon season. Another branch of the strong current along the coast of Sri Lanka travels in a north-northeasterly direction along the east coast of India. This current later moves south and then in the west direction to complete the anticyclonic gyre in the central part of the model area. A strong northward flowing western boundary current was observed along the east coast of Sri Lanka and India. A weak southward flow was observed along the northeast coast of India. The simulated circulation pattern towards the end of July (figure 8) was analogous to that of the previous month, the only difference being that the intensity of the cyclonic eddy formed at the northeastern part of the Bay was reduced. The high magnitudes of currents at the southwest corner of the model area may be associated with the clamped boundary condition $\eta = 0$ imposed along the southern boundary.

CS charts for the period 10–20 July (figure 9) show, in general, north-northeastward flow with magnitude of less than 40 cm/s along the east coast of India. One large anticyclonic gyre in the central region and a narrower one in the southern region

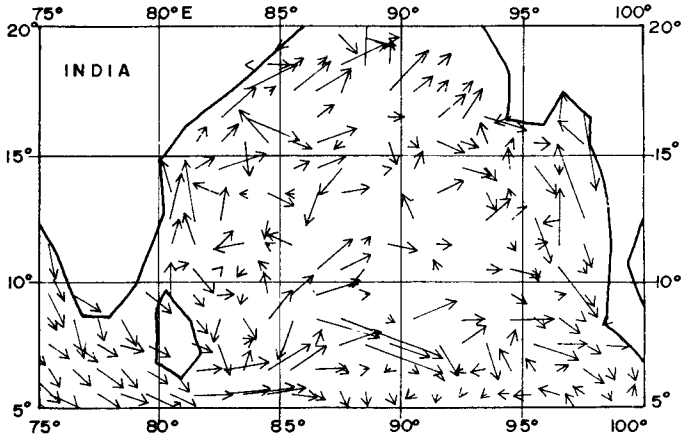

Figure 9. Observed ship drift for the period 20–30 July (Cutler and Swallow 1984).

can be seen in this chart which is comparable to the present model simulations. The magnitude of computed currents is less than surface drift currents mainly because the computed currents are depth-averaged. We could only make some gross comparison of our model results with ship drift data which are just the compilation of 60 years of data, collected randomly from the area. These data were neither filtered nor corrected for systematic sampling errors. Therefore, the exact extent or size of the gyres simulated could not be compared with ship drift data. We attempted a comparison of our simulation results with the model studies of Cox (1970). Cox's model analysis gave the circulation pattern for the August and February months in the Indian Ocean area and it could not resolve any of the eddies or gyres found in BB. In fact, the Bay of Bengal circulation was represented by just two arrows in Cox's model. A larger portion of its discussion was devoted to the large-scale dynamics of Arabian Sea.

5.2 *Northeast monsoon season*

The simulated currents towards the end of November and December are shown in figures 10 and 11 respectively. By 30th November, the northeast monsoon is fully set and the wind direction is northerly and northeasterly throughout the model domain. A large cyclonic gyre covering the central and western parts of the BB is formed during November. It appears like a step-like system over the central longitude with a northward current turning westward and then southward on approaching the east coast of India. The southward flowing coastal current along the east coast of India is the locally wind-driven western boundary current during the northeast monsoon season. Another weak anticyclonic gyre is found in the northern part of the BB. By 30th December (figure 11), the large cyclonic gyre, formed in the central and western parts, gets shifted towards south and gets more intensified. Other features of circulation during December are analogous to those of the previous months.

During November a well-defined cyclonic circulation covering the central and western parts of Bay of Bengal is formed (KNMI 1952). Our model simulation results alos show the presence of such a cyclonic circulation. However, the shipt drift data averaged for the period 10–20 December (figure 12) do not show the existence of

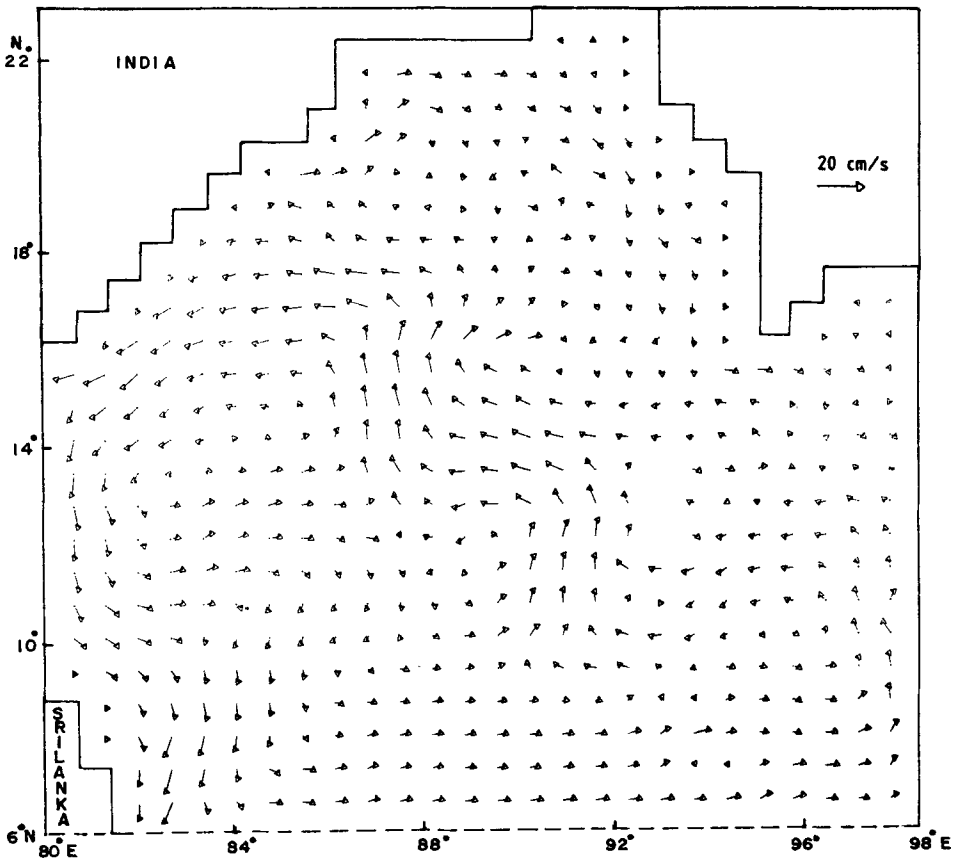

Figure 10. Simulated depth-mean currents for 30 November.

such a cyclonic circulation in the central and western parts of BB. The ship drift shows a strong southward moving western boundary current along the east coast of India and westward flow elsewhere in the domain.

In the simulation results, the western boundary current is found to be southward during November and December. This coastal current reverses its direction of flow during the southwest monsoon season. We, therefore, presume that the western boundary current along the east coast of India is locally wind-driven. It has also been observed that this western boundary current is more intense during the northeast monsoon season.

6. Summary and conclusions

We have shown that the depth-averaged seasonal circulation in the upper layers of BBAS can be simulated fairly accurately by means of a vertically-integrated hydrodynamic model. The present study is an attempt to numerically simulate the depth-mean circulation in the model area. Since the wind stress components are the main forcings in the model, an analysis of their distribution was also carried out. The

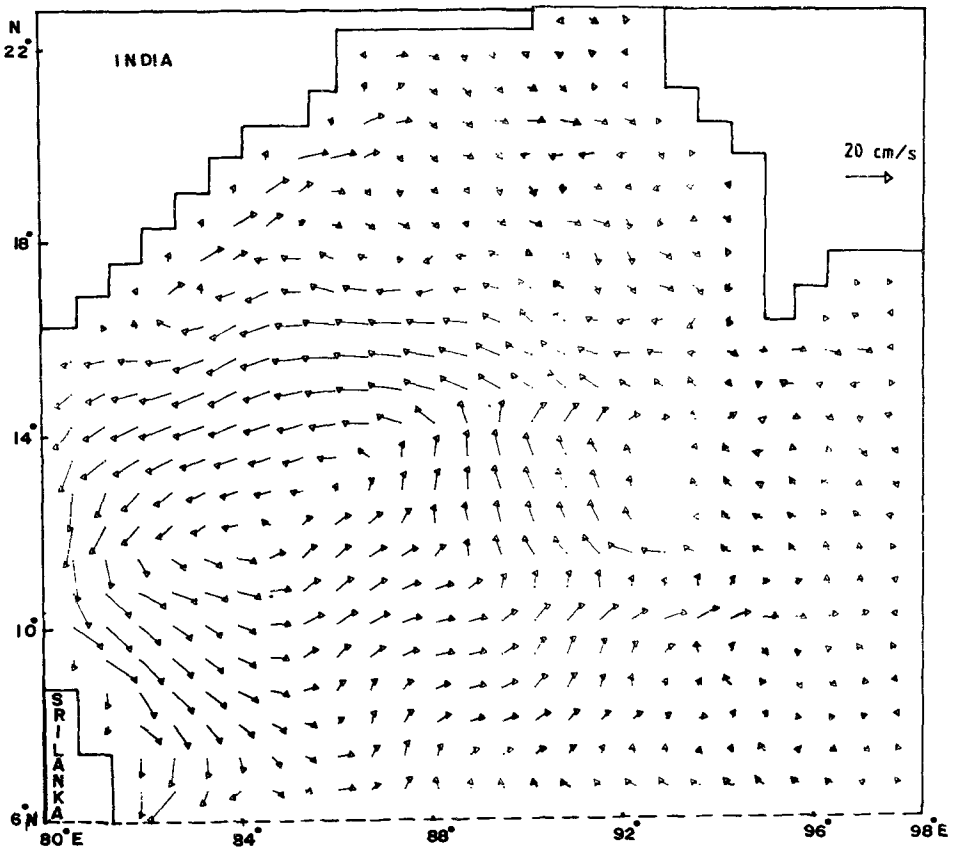

Figure 11. Simulated depth-mean currents for 31 December.

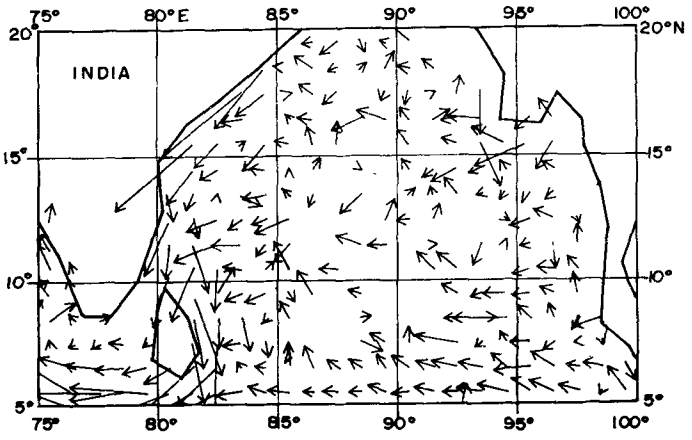

Figure 12. Observed ship drift for the period 20–30 December (Cutler and Swallow 1984).

model was tested with two types of open boundary conditions, one by applying a radiation type (equation (5)) condition and another by prescribing zero-surface elevation along the open boundary. Simulation results obtained by prescribing zero

sea surface elevation along the open boundary were found to be more realistic near the boundary, while in the interior part of the domain, the results of both the experiments were analogous.

A comparison of the model simulation results during two different seasons with the available information on currents (atlases in the form of surface drift charts) in the region shows that the model reproduces well the important features of circulation during different seasons. However, the magnitudes of simulated currents were found to be less than those observed at the surface. This is expected to a good extent, since the simulated currents are averaged over the upper Ekman layer. The model has been found to be successful in simulating the gyre type of circulation found in specific regions, the north equatorial current near the southern boundary during the northeast monsoon season and also the eastward moving monsoon drift current during the southwest monsoon season. During the southwest monsoon season, two anticylonic gyres were observed in the central and the parts of BB. The circulation during the northeast monsoon period was characterized by the presence of a large cyclonic gyre covering the central and western parts of BB. The simulated western boundary current along the east coast of India flows northward and southward during the southwest and northeast monsoon seasons respectively and we presume that it is locally wind-driven. Since there has so far been no systematic long-term observational programme for the Bay of Bengal it is difficult to validate all the findings of our model studies. These model simulation results may be useful for planning future observational programmes for the Bay of Bengal area.

Acknowledgements

The authors thank Drs B N Desai and J S Sastry for their keen interest and encouragement during the course of this study. The numerical computations were carried out on the ND-500 computer of this Institute and the help rendered by the staff of the Computer Division is also acknowledged.

References

Bahulayan N and Varadachari V V R 1986 Numerical model of wind driven circulation in the Bay of Bengal; *Indian J. Mar. Sci.* **15** 8–12

Cox M D 1970 A mathematical model of the Indian ocean; *Deep Sea Res.* **17** 47–75

Cutler A N and Swallow J C 1984 Surface currents of the Indian Ocean (to 25°S, 100°E) computed from historical data archived by meteorological office, Broadchell, UK; Institute of Oceanographic Sciences, Report no. 187, 81

Fandry C B 1981 Development of a numerical model of tidal and wind driven circulation in the Bass strait; *Aust. J. Mar. Freshw. Res.* **32** 9–29

Fandry C B 1982 A numerical model of the wind-driven transient motion in the Bass strait; *J. Geophys. Res.* **87** 499–517

Hastenrath S and Lamb P J 1979 *Climatic atlas of the Indian Ocean. Part I: Surface climate and atmospheric circulation* (University of Wisconsin Press) pp 97

Heaps N S 1973 Three-dimensional model of the Irish Sea; *Geophys. J. R. Astro. Sec.* **35** 99–120

Johns B, Dube S K, Mohanty U C and Sinha P C 1981 Numerical simulation of surge generated by Andhra cyclone; *Q. J. R. Meteorol. Soc.* **107** 919–934

KNMI 1952 Koninklijk Netherlands Meteorological Institute, Indian Ocean, Oceanographic and Meteorological data, Publication No. 135, 2nd ed.

Lafond E C 1958 On the circulation of the surface layers of the East coast of India; *Andhra University Memoirs in oceanography. Vol. II Andhra University, Series* **62** 1–11

Lafond E C and Boreswara Rao C 1954 Rotary currents in the Bay of Bengal; *Andhra University Memoirs in oceanography, Vol I Andhra University Series* **49** 102–108

Lafond E C and Lafond K G 1968 Studies of Oceanic circulation in the Bay of Bengal; *Bull. Natl. Inst. Sci. India* **38** 164–183

Legeckis R 1987 Satellite observations of a western boundary current in the Bay of Bengal; *J. Geophys. Res.* **92** 12974–12978

Luther M E and O'Brien J J 1985 A model of seasonal circulation forced by observed winds; *Progr. Oceanogr.* **14** 353–385

Meehl G A 1980 Observed ocean seasonal surface currents on a 5° grid; NCAR Technical Note-NCAR-TN/1A-159+STR

Murty T S 1984 Storm surges—Meteorological Ocean tides; *Can. Bull. Fish. Aq. Sci.* **212** 897–

Neumann V G 1974 Some features of Indian ocean surface current systems; *J. Mar. Biol. Assoc. India* **16** 367–370

O'Brien J J 1971 A two-dimensional model of the wind-driven circulation in North Pacific; *Invest Pesq.* **35** 331–349

Panakala Rao D and Sastry J S 1981 Circulation and distribution of some hydrographical properties during the late winter in the Bay of Bengal; *Mahasagar—Bull. Natl. Inst. Oceanogr.* **14** 1–15

Pond S and Pickard G L 1983 *Introductory dynamic oceanography* (Pergamon Press) 2nd ed., pp. 329

Shcherbinin A D, Arsenyev V S and Goldin Yu A 1979 The western boundary currents of the Bay of Bengal; *Dokl. Acad. Sci. USSR, Earth Sci. Soc.* (English translation) **244** 167–168

Varadachari V V R, Murty C S and Das P K 1968 On the level of least motion and circulation in the upper layers of the Bay of Bengal; *Bull. Natl. Inst. Sci. India Part I*, **38** 301–307

Wu J 1980 Wind stress coefficients over the sea surface near neutral conditions—a revisit; *J. Phys. Oceanogr.* **10** 727–740